Dependence of Polymer Thin Film Adhesion Energy on Cohesive Interactions between Chains

ARTICLE *in* MACROMOLECULES · AUGUST 2014

Impact Factor: 5.8 · DOI: 10.1021/ma5006974

3 AUTHORS:

Wenjie Xia
Northwestern University
12 PUBLICATIONS **76** CITATIONS
SEE PROFILE

David D. Hsu
Northwestern University
5 PUBLICATIONS **28** CITATIONS
SEE PROFILE

Sinan Keten
Northwestern University
75 PUBLICATIONS **1,471** CITATIONS
SEE PROFILE

Macromolecules

Article

pubs.acs.org/Macromolecules

Dependence of Polymer Thin Film Adhesion Energy on Cohesive Interactions between Chains

Wenjie Xia,[†] David D. Hsu,[‡] and Sinan Keten*[,†,‡]

[†]Department of Civil & Environmental Engineering, Northwestern University, 2145 Sheridan Road, Evanston, Illinois 60208-3109, United States

[‡]Department of Mechanical Engineering, Northwestern University, 2145 Sheridan Road, Evanston, Illinois 60208-3109, United States

ABSTRACT: Substrate−film interfacial properties play a fundamental role in the adhesion of glassy polymer thin films onto supporting substrates. Utilizing steered molecular dynamics (SMD) simulations, here we uncover that the cohesive noncovalent forces between polymer chains also have a significant effect on the adhesive properties of polymer films in contact with flat substrates. We demonstrate that weaker interchain interactions, all else being the same, can induce higher adhesion energy within the interface. Three different regimes in the adhesion energy profile can be characterized by a nonlinear scaling relationship. In the weak substrate−film interaction regime, the adhesion energy of the film exhibits near independence of cohesive force variations, and the entropic contributions to the surface free energy are consequential. In the intermediate regime, films with weaker cohesive forces exhibit higher adhesion energy due to the ability of polymer chains to pack more effectively in the interfacial region, thereby increasing the adhesive interaction density. In the strong interaction regime, the adhesion energy increases linearly with the adhesive interaction strength because of saturation of local packing in the interfacial region. These findings corroborate recent polymer dewetting observations that have hinted on the importance of local relaxation and packing effects on interfacial properties.

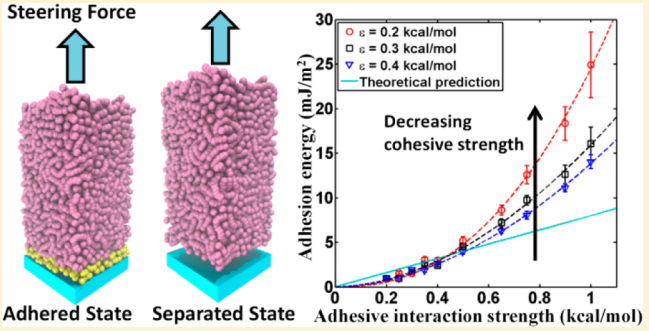

INTRODUCTION

Polymer thin films play an increasingly important role in a wide array of applications in the field of nanotechnology and bioengineering, such as within nanoelectronics,[1,2] nanocomposites,[3,4] coatings,[5] and biocompatible devices.[6] Beyond the importance of their technological function, thin film model of bilayer systems have also been shown to exhibit thermomechanical behavior and nanoscale interface phenomena analogous to those seen in nanocomposite materials.[7,8] Understanding the fundamental mechanisms of polymer adhesion and wetting at the molecular level is of critical importance as it governs failure mechanisms and thermomechanical properties of the deposited films.

Recent studies suggest that the adhesion energy of polymer films is influenced not only by the noncovalent interfacial force between the polymer and substrate, but also by the strength of the cohesive interactions within the film itself. The relative roles of these interactions on adhesion energy at the nanoscale, however, have not been previously explained. Here we define adhesion energy as the work required to separate the film from the substrate and create two free surfaces. We focus our effort on investigating the adhesion of glassy polymer thin films, where the difference between the energy of bound and unbound surfaces are sought after.

Earlier efforts have been focused on quantitatively describing the molecular origins of polymer adherence to a rigid, solid, and impermeable substrate upon thin film deposition. It is believed that the nanoscale interfacial layer, or the so-called "interphase" in nanocomposites, exhibits conformational and dynamical differences when compared to the bulk properties of the polymer. The stark differences observed for interphase regions are often attributed to local variations in the segmental mobility and structural relaxation of polymer chains.[9−11] Such changes are caused by the surface potential of the substrate, and the extent of the ability of the surface potential to perturb the film structure in return governs its adhesion mechanism. Unlike single chain adsorption onto surfaces, the adhesive interactions within the substrate−film interface must depend on the cohesive interactions and steric hindrances between chains. For example, experiments and simulation indicate that when the cohesive behavior within a polymer film are modified by the inclusion of small molecules in thin film composites or by varying the side-chain chemistry, the ability of a polymer film to adhere to the substrate is affected due to a shift in the chain relaxation mechanism and energy dissipation.[12−14] Additionally, the adhesion energy of a polymer film under confinement is closely related with the glass-transition temperature (T_g), which is a key characteristic that governs the thermomechanical

Received: April 3, 2014
Revised: May 27, 2014
Published: July 18, 2014

   dx.doi.org/10.1021/ma5006974 | *Macromolecules* 2014, 47, 5286−5294

properties of the polymer film. On one hand, the T_g of the film can either increase or decrease depending on the relative interaction strength between the film and substrate;[15−17] on the other hand, with the same surface potential, the film with lower T_g can induce higher adhesion energy.[18]

Recent experimental and simulation studies have shown that strong interaction strength between the film and surface are not enough to induce "sticky" behavior at the macroscopic scale due to surface roughness effects which reduce the area of contact. Weaker cohesive interaction strength in the film material (such as in adhesives) can directly affect the subsequent adhesion energy by varying the degree of compliance of the film to the rough surface, which in turn increases the effective contact area.[19−21] It is not well-understood whether similar effects can be observed in polymer films on "exceptionally smooth surfaces" such as silicon or nanocrystal substrates where the surface at the molecular and nanoscales can be taken to be atomically flat. Bilayer systems of this kind are relevant for numerous applications including photoresists, as well as nanocomposites with graphene, or atomically flat nanocrystals. Polymer films in these applications can be brought in close contact using spin-casting and annealing in a clean room environment, and therefore can be assumed to have near perfect contact with a flat surface.[19,22]

Measurements of adhesive properties and surface forces have been performed using various techniques in nano and microscale experiments, however, simulations of idealized models are necessary in elucidating mechanisms of adhesion of glassy polymers at the molecular scale. Experimental methods can be sorted into two types: (1) direct measurement, as often obtained by atomic force microscopy (AFM),[23] surface force apparatus (SFA),[24] optical trapping (OT),[25,26] and other techniques;[27,28] (2) indirect measurements, including compressibility cell and osmotic pressure methods.[29,30] While it is relatively straightforward to examine single-chain adhesion onto surfaces,[31−35] it is not clear how one can translate comparative measurements at the single chain level to the adhesion of a thin film made up of the same polymer. Molecular simulations could provide this link by allowing higher control of system configurations and high fidelity in the observed quantities of interest by simultaneously capturing chain statistics during the separation process. Steered molecular dynamics (SMD) simulations[36−39] and surface energy approaches based on the Young−Dupre equation[40] are particularly useful for this purpose because they can provide mechanistic insight by enabling manipulation of a glassy film and allowing inspection of the chain relaxation and conformational behavior of the film at the interfacial layer. The obtained energetic relationships can then inform traction−separation laws commonly used in continuum mechanics for describing interfacial mechanics.

In the present study, we investigate the interrelation between adhesive and cohesive interactions in supported thin films, and the adhesion energy dependence under these two factors. Cohesive interaction between chains in experiments can be varied through by side-chain functionalization, incorporation of plasticizing/antiplasticizing agents, and other approaches. Idealization of such effects can be done using atomistically informed coarse-grained molecular dynamics simulations by systematically varying the cohesive interaction strength independently from adhesive interactions with the solid substrate. SMD simulations used to separate the film−substrate interface, as well as energetic considerations reveal that the adhesive and cohesive forces have significant influence on the adhesion energy below the glass-transition temperature of the film. Correlations of the adhesion energy with conformational changes that occur within the film during the simulated separation process provide new insight into both energetic as well as entropic effects on adhesion.

METHODS

Coarse-Grained Model Development. The coarse-grained potential terms are parametrized based on the all atomistic simulations of poly(methyl methacrylate) (PMMA). The bond stretching and angle bending interactions in the CG model are developed by matching them to respective atomistic probability distribution function using the inverse Boltzmann method.[41,42] Each force and mass center of coarse-grained beads in the model represents a repeat unit, and is at the central carbon site in the backbone as indicated in Figure 1a. We

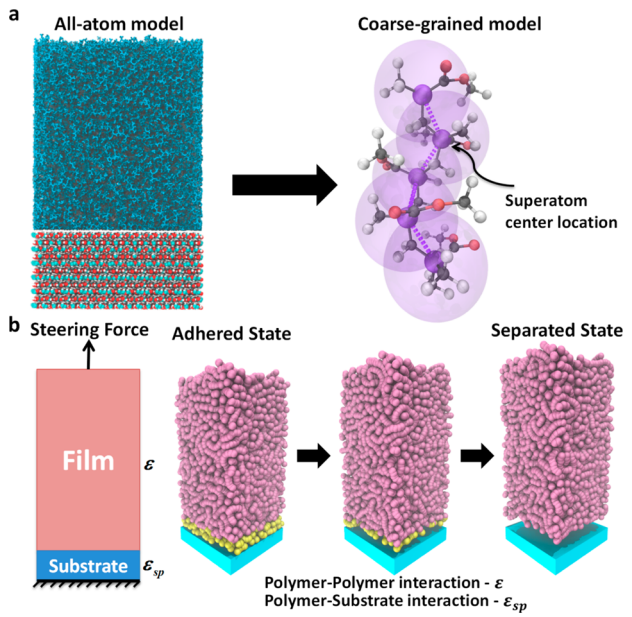

Figure 1. (a) Example of an all-atom PMMA thin film model adhered to a cellulose nanocrystal substrate, and the mapping from the all-atom model to the one-bead coarse-grained model. (b) (Left) Schematic illustration of a supported polymer thin film subjected to a steering force. (Right) Coarse-grained MD simulation snapshots during the steering process. The beads within the cutoff range (15 Å) of the attraction of the substrate are labeled in yellow.

employ a Lennard-Jones (LJ) 12-6 potential to define cohesive nonbonded interactions for both intrachain and interchain interactions between CG atoms, excluding the nearest bonded neighbors

$$U_{LJ} = 4\varepsilon\left[\left(\frac{\sigma}{r}\right)^{12} - \left(\frac{\sigma}{r}\right)^{6}\right], \quad r \le r_c \tag{1}$$

where ε is the depth of the potential well and signifies the cohesive interaction strength and σ is the point at which the potential crosses the zero energy line. These two parameters are calibrated to match the experimental density at room temperature and T_g of bulk PMMA. The resulting values of σ and ε are 6.5 Å and 0.3 kcal/mol, respectively, which yield a density of 1.17 g/cm^3 and bulk T_g of 388.6 K. The cutoff distance of the nonbonded potential r_c is 15 Å. Moreover, the CG model is validated by the experimental Flory−Fox constants of PMMA that define molecular weight dependence of bulk T_g, which our model readily captures with no additional empirical input. Starting from this basic CG model, we systematically vary the cohesive interaction strength ε from 0.2 to 0.4 kcal/mol, while keeping σ constant for all simulations, as described in our previous study.[18] Hence, by varying the ε value, we are able to explore the dependence of the adhesion

dx.doi.org/10.1021/ma5006974 | Macromolecules 2014, 47, 5286−5294

energy on the cohesive interaction strength of the polymer film, using the existing CG model as a representative polymer structure. We note that as the ε value is varied from the calibrated CG value, the model is no longer necessarily representative of PMMA, and is rather used as a generic polymer model. The details of the coarse-grained model can be found in our earlier study.[16]

Polymer Thin Film Configuration. CGMD thin film simulations are carried out using 100 chains with 100 repeat units each, resulting in a thin film with ∼18 nm thickness at room temperature. Periodic boundary conditions of the simulation cell are applied only in the $x-y$ plane which is generated with an area of 9 nm × 9 nm. The z dimension of the simulation box is nonperiodic and is much larger than the film thickness in order to simulate a free upper surface. To simulate the film−substrate adhesive interaction at the bottom surface, we introduce an implicit wall interacting with the film using a truncated Lennard-Jones (LJ) 12-6 potential:

$$E_{sub}(z) = 4\varepsilon_{sp}\left[\left(\frac{\sigma_{sub}}{z}\right)^{12} - \left(\frac{\sigma_{sub}}{z}\right)^{6}\right], \quad z \le z_c \tag{2}$$

where z denotes the distance from the bead to the wall, ε_{sp} affects the depth of the potential well and denotes the substrate−film adhesive interaction strength which is varied from 0 to 10.00 kcal/mol in our study. The limiting case of ε_{sp} = 0 kcal/mol represents a free-standing film with two free surfaces. σ_{sub} is the distance from the substrate at which E_{sub} crosses the zero axis. The cutoff of the interaction z_c is 15 Å. We elect to use the 12-6 form to maintain the same definition of potential terms for both cohesive interaction strength ε and substrate−film adhesive interaction strength ε_{sp}, which allows for easier intermolecular force comparison.

Glass Transition Calculation. The glass transition temperatures T_g of both bulk and film samples are determined using the method described by Tsige and Taylor.[43] With this method, the time-dependent mean-squared displacement (MSD) of all beads are measured at 20 K intervals from 530 to 190 K. This provides a metric of molecular mobility as a function of temperature, which undergoes a characteristic change of slope at the onset of glass transition. The time-averaged values of MSD from 10 to 2000 ps are plotted as a function of temperature. The MSD data in the lower temperature region and the higher temperature region are fitted linearly, and the intersection of these two lines indicates the T_g as shown in Figure 2.

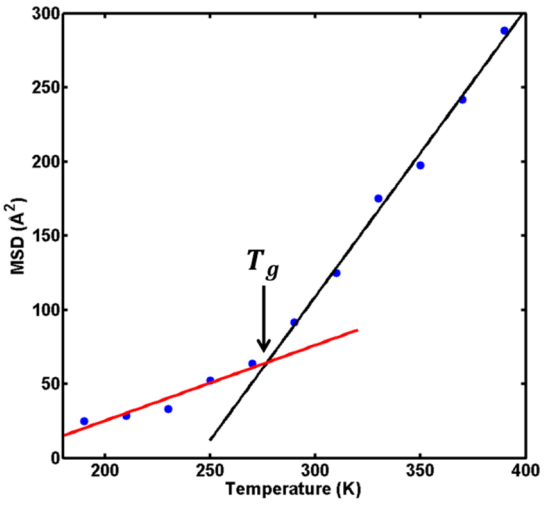

Figure 2. T_g prediction of the free-standing film with the cohesive interaction strength ε = 0.2 kcal/mol via the measurement of mean-squared displacement (MSD) of CG atoms at different temperatures. MSD data in lower temperature region and higher temperature region is fitted by linear lines. The intersection of the slopes is predictive of T_g.

Calculation Methods for Adhesion Energy. The adhesion energy between the film and the substrate is investigated by employing the steered molecular dynamics (SMD) approach. In our simulations, the film is peeled from the fixed substrate by applying a steering force generated by a stiff spring tethered to the film (Figure 1b). The potential generated by the harmonic spring has the form: $U_{smd}(t) = 1/2k[vt - (R(t) - R_0)]^2$, where R_0 is the initial equilibrium position of the center of mass (COM) of the film and $R(t)$ is the current position of the COM of the film in the pulling process. Each monomer is individually subjected to a restoring force with a magnitude of $k[vt - R(t) - R_0]m_i/m$, where m_i is the mass of each bead and m is the total mass of the film. This effectively constrains the center of mass of the film to move with the constraint, while allowing relaxation processes to occur within the film during the deformation. The pulling rate v is kept constant and is selected to be 0.5 m/s. The pulling force is normal to the substrate and the spring constant k is chosen to be 200 kcal/mol Å^2. Simulations are performed after equilibration for 10 ns under the canonical ensemble (NVT). The work done in separating the two surfaces are averaged over multiple configurations based on Jarzynski's equality,[39,44,45] which yields an estimate of the potential of mean force (PMF) of an interface from a nonequilibrium process.

The free energy landscape as a function of the chosen coordinate, which is also known as the potential of mean force (PMF),[46] can be evaluated based on the following equation:

$$\mathrm{PMF} = -\frac{1}{\beta}\log\langle e^{-\beta W}\rangle \tag{3}$$

where β is equal to $1/(k_BT)$ in which k_B is the Boltzmann constant and T is the temperature, W is the sampled work from ten different trajectories during the pulling process, and $\langle ...\rangle$ denotes the ensemble average. The pulling rate is selected to be in the regime where the PMF measurement is observed to be independent of the pulling rate. Each SMD simulation is run for 1.2 ns with a time step of 4 fs. The adhesion energy w is obtained by taking the free energy difference between the PMF at the equilibrium distance at the initial adhered state F_{ad} and the final, fully separated state F_{sep} at a large distance, which is equal to the plateau value of the PMF divided by interfacial area A:

$$w = \Delta F = F_{sep} - F_{ad} = \frac{\mathrm{PMF}^{plateau}}{A} \tag{4}$$

Assuming no changes occur in the film compared to the bulk during the adhesion and separation process, the internal adhesion energy of the supported thin film system can also be calculated by directly summing the potential energy between the polymer beads and the substrate based on eq 2, which we call the direct energy summation (DES) approach. The difference between the energy calculations by SMD and DES approaches is that SMD takes into account the configurational entropic contributions associated with adhesion, whereas the DES approach only includes the energetic contribution. The comparison of the calculations by the SMD and DES approaches can provide insight into the role of entropy and local density changes in the total adhesion energy in thin films.

It should be noted that at very large values of the substrate−film attraction strength, cohesive fracture occurs within the film during the SMD peeling process. Here we focus on cases where a clean interface is formed in the peeling process without a larger fracture process zone. Peeling with a clean interface occurs in the range ∼0.2 < ε_{sp} < ∼1.0 kcal/mol in the SMD simulations. In the DES approach, the adhesion energy calculation does not rely on physical pulling simulations, and therefore summation of energies can be carried out for a larger range of ε_{sp}, which we vary from 0.20 to 10.00 kcal/mol.

RESULTS AND DISCUSSION

To put our results into a more generalized context, we first characterize how the glass-transition temperature T_g of the polymer changes as the cohesive interaction strength (ε) is varied. This is done for both a bulk polymer model with

dx.doi.org/10.1021/ma5006974 | Macromolecules 2014, 47, 5286−5294

periodic boundary conditions in all directions, as well as an 18 nm-thick free-standing film, where no substrate is present. It is well-known that nanoscale free and substrate surfaces influence the T_g of polymer thin films (T_g^{film}) in comparison to the bulk T_g of the polymer. The simulation results show that both T_g^{bulk} and the free-standing film T_g^{film} increase with ε, which is the cohesive interaction strength between the chains (Table 1).

Table 1. Measured Glass-Transition Temperatures of Bulk Polymers (T_g^{bulk}) and 18 nm-Thick Free-Standing Films (T_g^{film}) for Different Cohesive Interaction Strength (ε)

ε (kcal/mol)	T_g^{bulk} (K)	T_g^{film} (K)
0.2	321.5 (±18.7)	282.6 (±8.8)
0.3	388.6 (±10.1)	363.3 (±8.6)
0.4	411.1 (±21.7)	401.1 (±10.4)

T_g^{film} is less than T_g^{bulk} for each ε, which can be attributed to the dominant effect of enhanced mobility induced by the free surfaces for this system.[47−49] In the limiting case where ε_{sp} is zero, surface interaction vanishes and the model becomes analogous to a free-standing thin film. As expected, a supported thin film with any nonzero value of ε_{sp} has a T_g^{film} that is always greater than that of the free-standing film due to the confining effect of the attractive solid substrate.

Next, we assess how the adhesion energy w between the polymer film and the substrate is influenced by the cohesive interaction strength ε and the substrate−film adhesive interaction strength ε_{sp}. Figure 3a illustrates the potential of mean force (PMF) obtained from pulling the film off the substrate orthogonally to the interfacial plane at 250 K. These results are for a polymer with ε = 0.3 kcal/mol. This temperature is at least ∼30 K below T_g^{film} in all of our simulations. Therefore, all of the films studied here are glassy and separate with clean interfaces. Thermal fluctuations at these low temperatures are not large enough to cause separation without an applied force.[50] The shape of the PMF curves for all ε_{sp} values can be characterized into three different regimes, which are typical of weakly interacting surfaces.[9,51−53] The first regime exhibits a quadratic dependence of pulling distance d for values below ∼1 Å, which is representative of a harmonic stretching force acting between the film and the substrate. The second regime exhibits a sublinear increase in PMF as a function of pulling distance. Once the film is fully detached from the substrate, a third regime is demonstrated where the slope of PMF curve (force of attraction) becomes zero and surfaces are fully separated.

Figure 3b provides an analysis of how the adhesion energy w varies with ε_{sp}, which is varied from 0.20 to 1.00 kcal/mol at different cohesive interaction strength values ε. We find that for each ε, the adhesion energy increases nonlinearly with ε_{sp}. To show the nonlinearity, we initially fit the data with a power law (dashed curves): $w \sim (\varepsilon_{sp}/\varepsilon)^a$, where α is a fitting scaling exponent obtained from the best fit. At lower values of ε_{sp} below ∼0.5 kcal/mol, there is no observable difference in the adhesion energy. As the adhesive interaction strength ε_{sp} is increased to be above ∼0.5 kcal/mol, the difference in w becomes increasingly large as ε is varied. Remarkably, films with a lower cohesive interaction strength ε are able to achieve a higher adhesion energy for the same ε_{sp}. In our simplified CG model, the film interacts with the substrate only through the van der Waals (vdW) interactions normal to the substrate surface. The collective substrate−film vdW interaction energy

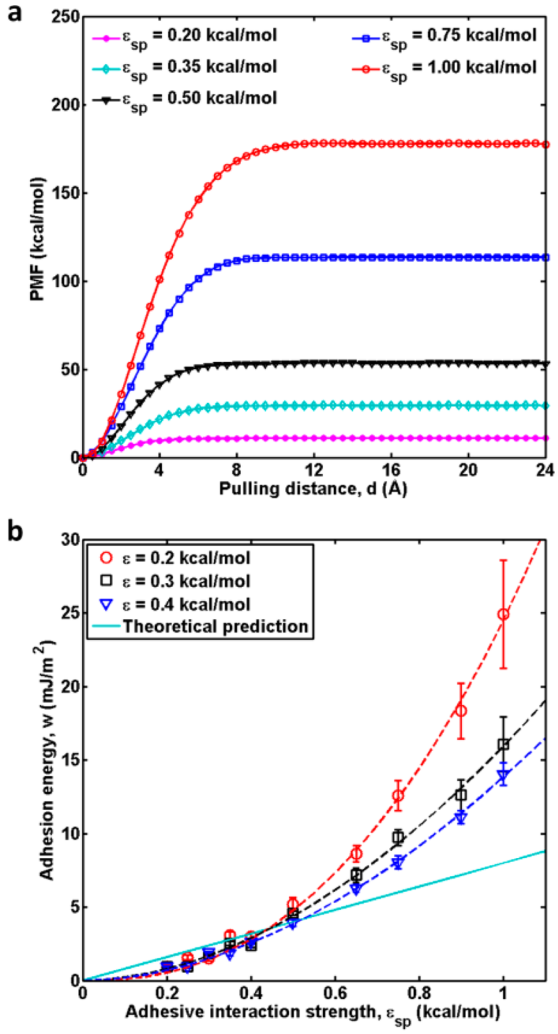

Figure 3. (a) Plot of the potential of mean force (PMF) as a function of pulling distance along the pathway in the pulling direction orthogonal to the substrate for supported polymer films with cohesive interaction ε = 0.3 kcal/mol and varying adhesive interaction strength ε_{sp} at T = 250 K. (b) The adhesion energy w as a function of adhesive interaction strength ε_{sp}, ranging from 0.20 to 1.00 kcal/mol, for varying cohesive interaction strength ε. The solid line shows the theoretical prediction as described by eq 6. The dotted lines correspond to the fits by the scaling relationship as described by a power law: $w \sim (\varepsilon_{sp}/\varepsilon)^a$. The fitted scaling exponent: α = 2.367 for ε = 0.2 kcal/mol, 1.865 for ε = 0.3 kcal/mol, and 1.848 for ε = 0.4 kcal/mol.

E_v due to this surface potential can be theoretically predicted based on a generalized form of the de Boer−Hamaker (dBH) model:[40,54,55]

$$E_v = -\int_D^\infty \rho^{film} E_{sub}(z)\, dz \tag{5}$$

where E_{sub} is the interaction potential between substrate and film as shown in eq 2, ρ^{film} is the number density of the film, and D is the equilibrium separation distance between the film and the substrate, which can be approximated as the distance where E_{sub} achieves a minimum value: $D \cong 2^{1/6}\sigma_{sub}$. To quantify what the adhesion energy would be under the condition that film properties are unperturbed by the surface properties, we assume that the film is homogeneous in terms of density and that the number density is equivalent to the bulk value ($\rho^{film} \cong \rho^{bulk}$), which yields

dx.doi.org/10.1021/ma5006974 | Macromolecules 2014, 47, 5286−5294

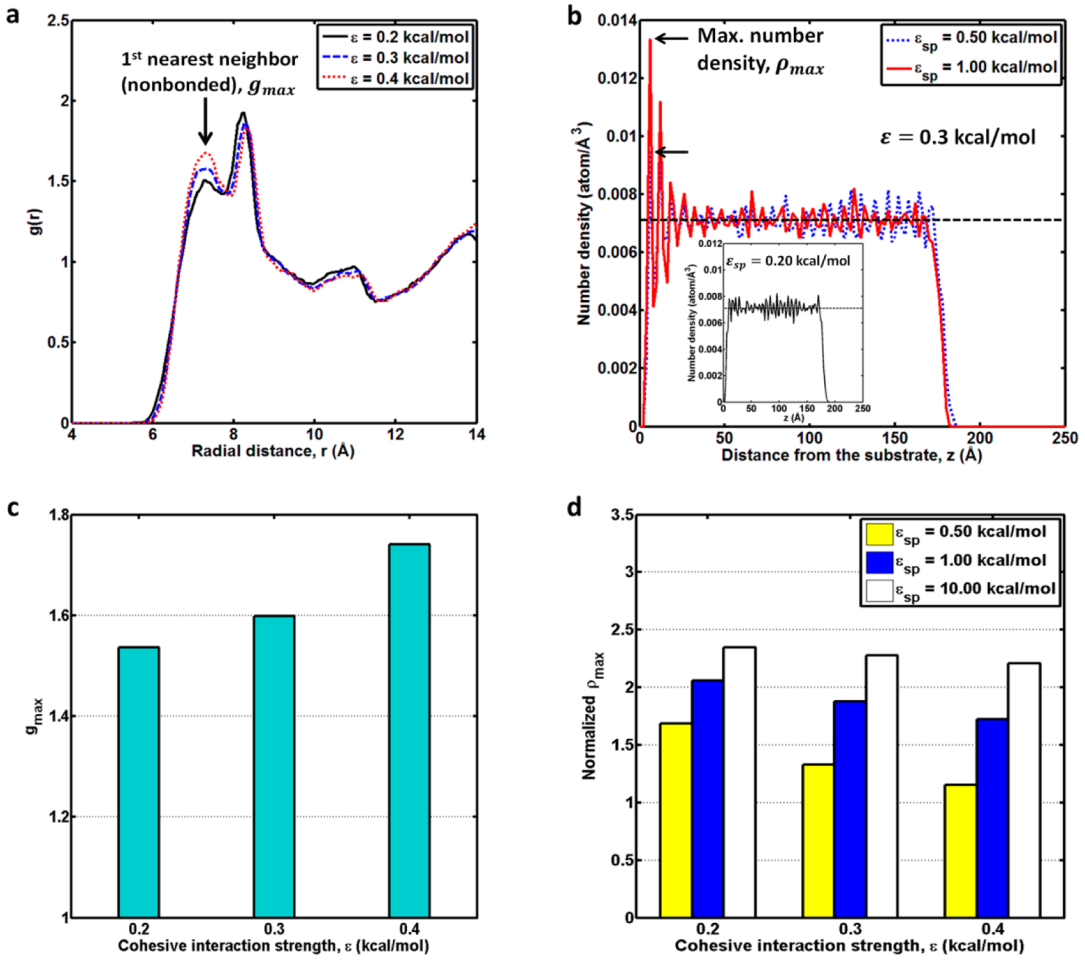

Figure 4. (a) Plot of radial distribution functions ($g(r)$) for bulk polymers with different cohesive interactions at T = 250 K. The first peaks of $g(r)$ curves denoted by the arrow indicate the 1st nonbonded nearest neighbor atoms (g_{max}). (b) Number density profile along the direction orthogonal to the substrate for ε = 0.3 kcal/mol at 250 K. The maximum number density ρ_{max} is defined as the peak value at the vicinity of substrate−film interface, which is marked by the arrows. The horizontal dashed lines indicate the bulk number density value of 0.0071 bead/Å^3. (Inset) Number density profile for weak adhesive interaction strength ε_{sp} = 0.20 kcal/mol. No peak is observed in this profile. Panels c and d show the results of g_{max} and normalized ρ_{max} (the ratio of ρ_{max} to the bulk number density).

$$E_v = -4\rho^{film}\left(\frac{\sigma_{sub}^{12}}{11D^{11}} - \frac{\sigma_{sub}^{6}}{5D^{5}}\right)\varepsilon_{sp} = C\varepsilon_{sp} \quad (6)$$

The vdW interaction energy E_v is shown to scale linearly with ε_{sp} as represented by the solid line in Figure 3b. The coefficient C is determined analytically to be 0.0115 Å^{-2} for our system. It should be noted that the form of eq 6 is different from the original dBH model because of the different substrate−film interaction potential used in our study. For the range of ε_{sp} below ∼0.5 kcal/mol, our simulation results are very close to the dBH model prediction that predicts a linear relationship with ε_{sp} and does not account for any dependence on the cohesive interaction strength ε. The agreement between the theory and simulations suggest that indeed the cohesive interaction does not influence the adhesion energy in this regime. However, in the range where ε_{sp} is above ∼0.5 kcal/mol, the adhesion energy deviates from the theoretical prediction, and also demonstrates a dependence on the cohesive interaction strength ε. This phenomenon, also observed in a recent study,[9] cannot be captured by the classical dBH model.

The key observation from these studies is that not only adhesive but also cohesive energy density influences the adhesive properties of the film when the surface potential is highly attractive. To explain this effect, we first examine whether the local structural changes in the film due to the presence of the surface plays a role in the adhesive properties. For this purpose, we quantify how the polymer packing in bulk and in thin films vary with cohesive interaction strength ε. This is done by computing the radial distribution function (RDF) $g(r)$ for the polymer chain monomer force centers in bulk, and number density profile near the substrate.

In Figure 4a, plots of the bulk RDFs exhibit two major peaks that indicate the preferred radial distances of the first and second nearest nonbonded neighbors from a reference CG bead. Since the RDF can be related to the nonbonded potential between the chains via a Boltzmann inversion,[56] it is expected that the greater depth of the nonbonded potential well ε can induce a higher $g(r)$ value of the first peak, which is denoted as g_{max}. The resulting g_{max} for systems with different ε values is shown in Figure 4c. Because of the excluded volume effect of polymer beads in the first neighbor shell, the $g(r)$ value of the second peak becomes lower as ε increases.

Figure 4b shows the number density profile across the film. The profile exhibits three different regions: an interfacial region with well-defined peak positions near the substrate, an interior

dx.doi.org/10.1021/ma5006974 | Macromolecules 2014, 47, 5286−5294

bulk-like region with an almost constant density close to the bulk value, and a free-surface region with lower density. The first peak in the profile is located at ~6 Å, which is denoted as ρ_{max}, the number density in the first layer of adsorbed CG beads. As the adhesive interaction strength decreases to lower values (e.g., ε_{sp} = 0.20 kcal/mol (inset)), this peak disappears. Figure 4d shows the comparison of the results of normalized ρ_{max} (the ratio of ρ_{max} to the bulk number density) for different values of ε_{sp} and ε. Two key features can be easily observed from the comparison of ρ_{max} with g_{max}. First, for all values of ε studied, ρ_{max} increases with the adhesive interaction strength ε_{sp}, marking a densification of the bulk polymer near the interface. Second, for all values of ε_{sp}, the ρ_{max} is greater for lower ε, which is in contrast with the decreasing trend of g_{max} from the bulk RDF in Figure 4c. This result indicates that the substrate induced densification effect on the interfacial structural properties is stronger for the polymer film with a lower cohesive interaction strength ε.

For ε_{sp} above ~0.50 kcal/mol, polymer segments with lower ε experience more ordering at the interfacial region close to the substrate, and achieve a more effective packing configuration. Higher local density gives rise to a greater adhesion energy. However, for weak confinement with ε_{sp} below ~0.50 kcal/mol, the substrate−film interaction strength is not strong enough to notably cause local ordering at the interface, and therefore the adhesion energy is nearly independent of ε. This analysis explains why dBH theory is a reasonable approximation for weakly adhering substrates. Additionally, the increment in ρ_{max} for each ε becomes less significant for ε_{sp} values above ~1.00 kcal/mol. It can be seen that the increase in ρ_{max} with increasing ε_{sp} from ε_{sp} = 0.50 to 1.00 kcal/mol is even slightly larger than that from ε_{sp} = 1.00 to 10.00 kcal/mol, which implies a saturation of local density at very large ε_{sp} values. These results are corroborated by recent experiments and simulations, which have consistently suggested that the adhesive properties of supported film are strongly affected by the change of the local structures of the first several atomic layers at the vicinity of the substrate.[9,12,57]

Next, we build upon this analysis of the density changes in the film and generalize their effects on the adhesion energy w of thin films. Figure 5 illustrates three qualitatively distinct regimes for w versus ε_{sp}. Regime I is characterized by the region where ε_{sp} is lower than ~0.5 kcal/mol. In this regime, w values obtained from the theoretical dBH equation, direct energy summation (DES) method, and SMD diverge. For lower values of ε_{sp}, the DES method estimates slightly higher adhesion energy than the PMF calculated from SMD simulations. This is because as the film is separated from the substrate in the SMD simulation, polymer chains at the interface undergo favorable conformational rearrangement. The DES calculation does not take the rearrangement into account. This effect can be quantified by considering the conformational changes of the polymer chains in the films as they are separated from the surface.

The conformational change of polymer chains due to relaxation upon dewetting the surface can be reflected by the shift of the mean value of the probability distribution function (PDF) of the radius of gyration R_g of polymer chains from a higher value in the adhered state to a lower value in the separated state (free-standing film), indicating an entropic penalty upon binding. This can be seen in Figure 6a, which shows the PDF of the R_g of polymer chains within the film as a function of ε_{sp}. The mean value and the standard deviation of

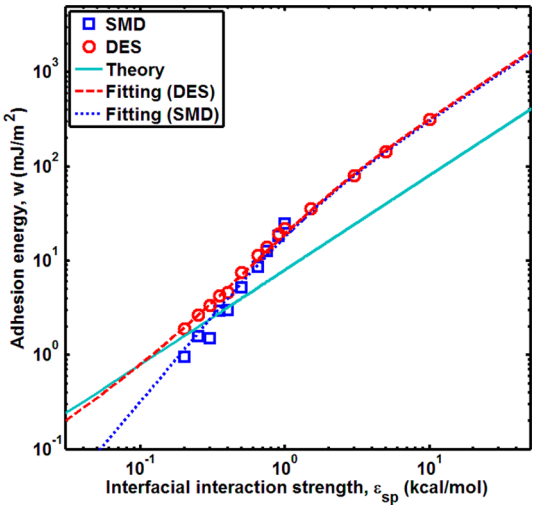

Figure 5. Results of the adhesion energy w obtained from the steered molecular dynamics (SMD) simulations (the same data as shown in Figure 3b) and direct energy summation (DES) as a function of adhesive interaction strength ε_{sp}, ranging from 0.20 to 10.00 kcal/mol, for the cohesive interaction ε = 0.2 kcal/mol. The solid line shows the theoretical prediction without accounting for the film density variation. The dashed and dotted curves show the fitting results for the DES data and the SMD data using the fitting formula as described by eq 7, which achieve R^2 values of 0.999 and 0.997, respectively.

PDF curves both increase with ε_{sp} in the adhered state, which indicates a stronger interfacial confinement effect induced by the substrate, which is supported by simulation and experimental observations.[58−60] This is also illustrated in Figure 6b, which shows the lower entropy "pancake" conformational state during adhesion compared to the higher entropy in the coiled conformational state after detachment from the substrate. The adhesion energy predicted by the dBH model in the first regime is slightly lower than the DES method. This is due to the dBH assumption that the density of the film at the surface is equal to the bulk density, which is an underestimation of the contact layer density. However, in the limit of very low ε_{sp}, this trend shifts, and the DES estimated adhesion energy tends to be lower than the dBH prediction since the density at the contact layer decreases below the bulk state in the free-standing thin film state. Additionally, dBH also overestimates w compared to the SMD method at low ε_{sp} as it does not account for the confinement of chains during adhesion. We perform a rate dependence study in which we vary the pulling speed of separation and measure the corresponding effect on the adhesion energy calculation. We find that below a certain pulling rate of ~2 m/s, the estimated adhesion energy becomes nearly rate independent, and subsequently we use a pulling rate of 0.5 m/s for our study. Here we stress that our SMD pulling rate is slow enough to see conformational changes and relaxation behavior during separation at the interfacial layer, although the SMD separation may not be a reversible process. This relaxation behavior during separation accounts for the discrepancy between the DES and SMD estimated adhesion energies at low ε_{sp}.

As ε_{sp} increases, a second regime II (~0.5 < ε_{sp} < ~1.0 kcal/mol) can be defined where the adhesion energy obtained from both SMD and DES methods begins to be increasingly greater than the dBH predictions, characterized by a nonlinear increase compared with the linear prediction of dBH. This can be attributed to the increase in the local density with ε_{sp} at the

dx.doi.org/10.1021/ma5006974 | Macromolecules 2014, 47, 5286−5294

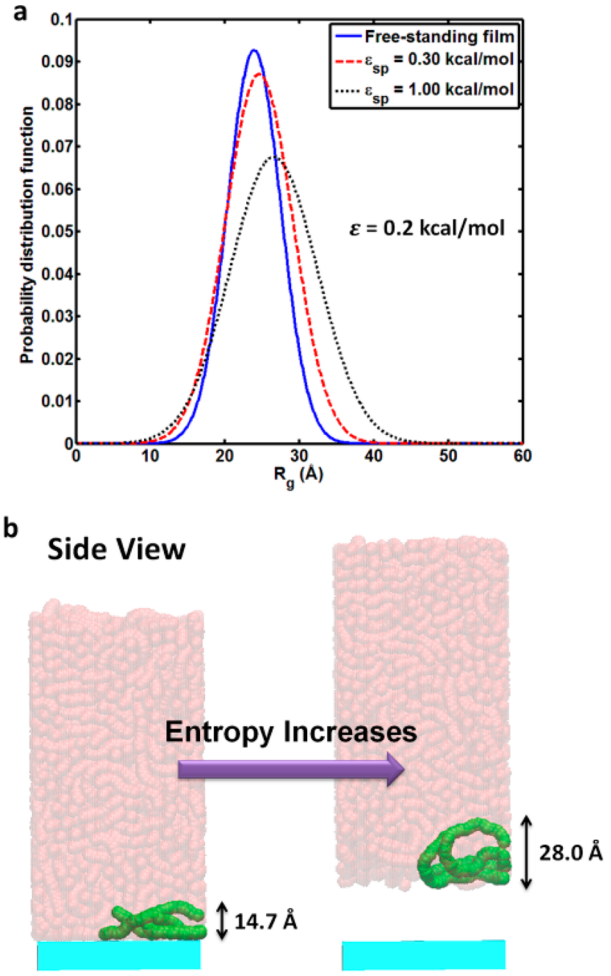

Figure 6. (a) Probability distribution function of the radius of gyration (R_g) of polymer chains in the film. (b) Snapshots of SMD simulations showing the conformational change of the polymer chain (colored in green) from the initial state where the film is attached to the substrate to the final state where the film is fully detached from the substrate. The conformation of the chain changes from the "pancake" shape to a coiled shape associated with an increase in the entropy.

interfacial region. Additionally, the SMD estimation of the adhesion energy begins to coincide with the DES curve, which indicates that the entropic contribution of the free energy becomes negligible compared with the energetic part as ε_{sp} increases.

Above this ε_{sp} threshold, we approach a third regime III for strong adhesive interaction strength ε_{sp} greater than ~1.0 kcal/mol, where the adhesion energy estimated by the DES method remains a linear function of ε_{sp}. In this regime, chains are so tightly packed due to the surface potential that they cannot reduce the free volume any further, which leads to a saturation of the attainable density.[9] Therefore, adhesion energy estimated by the DES method scales linearly with ε_{sp}. We note that SMD simulations predict that cohesive failure is also possible for ε_{sp} above ~1.0 kcal/mol and thus it is not possible to obtain a clean PMF for these cases. The qualitative behaviors of these three regimes allow us to better understand the strengths and limitations of each adhesion energy estimation method. For the cases in this regime, the DES method only considers adhesion energy of the interface but in real physical systems, cohesive failure and large process zones will require much larger work to separate these films from these surfaces.

In order to accurately capture the adhesion energy at a wide range of values of ε_{sp} on the basis of the dBH model, we apply a fitting function to describe the different behaviors of the three regimes with a single analytical functional form

$$w(\varepsilon_{sp}) = a\varepsilon_{sp} + b\left[1 - \exp\left(-\frac{\varepsilon_{sp}}{\varepsilon^*}\right)\right] \tag{7}$$

where a, b, and ε^* are fitting constants. In this functional form, at both the lower limit of ε_{sp} close to 0 kcal/mol and very large values above ~1.0 kcal/mol, w scales linearly with ε_{sp}:

$$\lim_{\varepsilon_{sp}\to 0} w = \left(a + \frac{b}{\varepsilon^*}\right)\varepsilon_{sp} \tag{8}$$

$$\lim_{\varepsilon_{sp}\to \infty} w = a\varepsilon_{sp} + b \tag{9}$$

In particular, when ε_{sp} approaches 0, the adhesion energy is expected to scale linearly with ε_{sp} since the density and entropic dependence are negligible at such low ε_{sp} (eq 8). Likewise, for large values of ε_{sp}, the adhesion energy is also expected to scale linearly with ε_{sp} after the density has saturated to a constant value (eq 9). For intermediate values of ε_{sp}, the adhesion energy is assumed to scale with some higher order function of ε_{sp} which we qualitatively capture with a smooth transition exponential term where ε^* in these cases can be related to the point at which the fitting model begins to deviate from the initial linear slope. All fitting equations agree reasonably well with the data in the range of the values studied. The fitting results are summarized in Table 2.

Table 2. Fitting Results of the Model (Eq 7) Used To Describe the Adhesion Energy Obtained from SMD and DES as a Function of Substrate−Film Adhesive Interaction Strength ε_{sp} for Cohesive Interaction Strength ε = 0.2 kcal/mol

	fitting parameters		
	a (Å^{-2})	b (kcal/mol Å^2)	ε^* (kcal/mol)
DES	0.048	−0.108	0.666
SMD	0.046	−0.098	0.516

Equation 7 captures some of the universal features of how glassy polymers with different cohesive energy density adhere to the substrate with varying adhesive interaction strength. However, we note that either very weak or very strong adhesive interactions may cause instability of film on the substrate in real applications due to dewetting or bond rupture of polymer at the interface. We also note that mechanisms of cohesive failure at high adhesive interactions can be much more complex, and one can expect deviation from the linear scaling relationship for the aforementioned reasons. Additionally, polymers above their glass-transition temperatures have not been the focus of this study as they are prone to cohesive failure, which causes measurement of adhesion energy to be more challenging. These effects could be studied further with SMD simulations that are designed to probe cohesive failure mechanisms.

CONCLUSION

We have systematically performed coarse-grained molecular dynamics simulations to investigate the adhesive and cohesive interaction effects on the adhesive behaviors of supported polymer films. By varying the substrate−film adhesive

dx.doi.org/10.1021/ma5006974 | Macromolecules 2014, 47, 5286−5294

interaction strength, we find that the adhesion energy of the film increases nonlinearly as a function of ε_{sp}, which is not captured by theoretical predictions. The cohesive interactions between polymer chains also play a critical role in determining the adhesive properties of the film. Our results show that the polymer film with a weaker cohesive interaction, all else being the same, can achieve stronger adhesion energy at large substrate−film adhesive interaction strengths. This is because when subjected to the substrate−film adhesive interaction, polymer structures with weaker cohesive forces have more conformational mobility and thus, pack more effectively at the interfacial region close to the substrate. Additionally, free energy contributions can be measured through SMD simulations in which the film is peeled off the substrate. We find that conformational entropy changes of polymer chains during separation cannot be ignored in accurately characterizing the adhesion energy for weak substrate−film interactions. However, at higher adhesive interaction strengths, the conformational entropy contributions to adhesion energy become negligible. In order to capture the adhesive behaviors over a wide range of adhesive interaction strengths, we propose an analytical fitting model to describe the adhesion data, which is well correlated with simulations. Our findings provide an explanation for recent experimental observations of substrate−film adhesion at the molecular level and pave the way for advancing film adhesive properties via interface nanoengineering.

AUTHOR INFORMATION

Corresponding Author

*(S.K.) Telephone: 847-491-5282, Email: s-keten@northwestern.edu.

Author Contributions

The manuscript was written through contributions of all authors. All authors have given approval to the final version of the manuscript.

Notes

The authors declare no competing financial interest.

ACKNOWLEDGMENTS

A supercomputing grant from Quest HPC System at Northwestern University is acknowledged. The authors acknowledge funding by the Army Research Office and Department of Civil & Environmental Engineering and Mechanical Engineering at Northwestern University.

REFERENCES

(1) Madou, M. *Fundamentals of microfabrication: the science of miniaturization*; CRC Press: Boca Raton, FL, 2002.
(2) Ito, H. *Microlithography—Molecular Imprinting* **2005**, *172*, 37−245.
(3) Ajayan, P. M.; Schadler, L. S.; Braun, P. V. *Nanocomposite Science and Technology*. Wiley: New York, 2006.
(4) Decher, G.; Schlenoff, J. B. *Multilayer thin films: sequential assembly of nanocomposite materials*. John Wiley & Sons: New York, 2006.
(5) Bertrand, P.; Jonas, A.; Laschewsky, A.; Legras, R. *Macromol. Rapid Commun.* **2000**, *21* (7), 319−348.
(6) Guire, P. E. *Biocompatible coating for solid surfaces*. US Patent 4,979,959, 1990.
(7) Rittigstein, P.; Priestley, R. D.; Broadbelt, L. J.; Torkelson, J. M. *Nat. Mater.* **2007**, *6* (4), 278−282.
(8) Schadler, L. *Nat. Mater.* **2007**, *6* (4), 257−258.
(9) Makeev, M. A.; Geubelle, P. H.; Sottos, N. R.; Kieffer, J. *ACS Appl. Mater. Interfaces* **2013**, *5* (11), 4702−4711.
(10) Hudzinskyy, D.; Lyulin, A. V.; Baljon, A. R. C.; Balabaev, N. K.; Michels, M. A. J. *Macromolecules* **2011**, *44* (7), 2299−2310.
(11) Tsuruta, H.; Fujii, Y.; Kai, N.; Kataoka, H.; Ishizone, T.; Doi, M.; Morita, H.; Tanaka, K. *Macromolecules* **2012**, *45* (11), 4643−4649.
(12) Zhang, C.; Hankett, J.; Chen, Z. *ACS Appl. Mater. Interfaces* **2012**, *4* (7), 3730−3737.
(13) Balzer, B. N.; Gallei, M.; Sondergeld, K.; Schindler, M.; Müller-Buschbaum, P.; Rehahn, M.; Hugel, T. *Macromolecules* **2013**, *46* (18), 7406−7414.
(14) Gersappe, D. *Phys. Rev. Lett.* **2002**, *89* (5), 058301.
(15) Fryer, D. S.; Peters, R. D.; Kim, E. J.; Tomaszewski, J. E.; de Pablo, J. J.; Nealey, P. F.; White, C. C.; Wu, W. L. *Macromolecules* **2001**, *34* (16), 5627−5634.
(16) Xia, W.; Mishra, S.; Keten, S. *Polymer* **2013**, *54* (21), 5942−5951.
(17) Priestley, R. D.; Mundra, M. K.; Barnett, N. J.; Broadbelt, L. J.; Torkelson, J. M. *Aust. J. Chem.* **2007**, *60* (10), 765−771.
(18) Xia, W.; Keten, S. *Langmuir* **2013**, *29* (41), 12730−12736.
(19) Pastewka, L.; Robbins, M. O. *Proc. Natl. Acad. Sci. U.S.A.* **2014**, *111* (9), 3298−3303.
(20) Akarapu, S.; Sharp, T.; Robbins, M. O. *Phys. Rev. Lett.* **2011**, *106* (20), 204301.
(21) Persson, B. N. J.; Tosatti, E. *J. Chem. Phys.* **2001**, *115* (12), 5597−5610.
(22) Tong, Q. Y.; Gosele, U. M. *Adv. Mater.* **1999**, *11* (17), 1409−1425.
(23) Binnig, G.; Quate, C. F.; Gerber, C. *Phys. Rev. Lett.* **1986**, *56* (9), 930−933.
(24) Israelachvili, J. N.; Adams, G. E. *J. Chem. Soc., Faraday Trans. 1* **1978**, *74*, 975−1001.
(25) Ashkin, A.; Dziedzic, J. M.; Yamane, T. *Nature* **1987**, *330* (6150), 769−771.
(26) Ashkin, A.; Dziedzic, J. M. *Science* **1987**, *235* (4795), 1517−1520.
(27) EssevazRoulet, B.; Bockelmann, U.; Heslot, F. *Proc. Natl. Acad. Sci. U.S.A.* **1997**, *94* (22), 11935−11940.
(28) Prieve, D. C.; Frej, N. A. *Langmuir* **1990**, *6* (2), 396−403.
(29) Homola, A.; Robertson, A. A. *J. Colloid Interface Sci.* **1976**, *54* (2), 286−297.
(30) Leneveu, D. M.; Rand, R. P.; Parsegian, V. A. *Nature* **1976**, *259* (5544), 601−603.
(31) Bhattacharya, S.; Rostiashvili, V. G.; Milchev, A.; Vilgis, T. A. *Phys. Rev. E* **2009**, *79* (3), 030802.
(32) Klushin, L. I.; Polotsky, A. A.; Hsu, H.-P.; Markelov, D. A.; Binder, K.; Skvortsov, A. M. *Phys. Rev. E* **2013**, *87* (2), 022604.
(33) Chervanyov, A. I.; Heinrich, G. *Phys. Rev. E* **2012**, *86* (3), 031801.
(34) Sebastian, K. L.; Rostiashvili, V. G.; Vilgis, T. A. *EPL (Europhys. Lett.)* **2011**, *95* (4), 48006.
(35) Horinek, D.; Serr, A.; Geisler, M.; Pirzer, T.; Slotta, U.; Lud, S. Q.; Garrido, J. A.; Scheibel, T.; Hugel, T.; Netz, R. R. *Proc. Natl. Acad. Sci. U.S.A.* **2008**, *105* (8), 2842−2847.
(36) Isralewitz, B.; Gao, M.; Schulten, K. *Curr. Opin. Struct. Biol.* **2001**, *11* (2), 224−230.
(37) Lu, H.; Isralewitz, B.; Krammer, A.; Vogel, V.; Schulten, K. *Biophys. J.* **1998**, *75* (2), 662−671.
(38) Keten, S.; Buehler, M. J. *Nano Lett.* **2008**, *8* (2), 743−748.
(39) Park, S.; Khalili-Araghi, F.; Tajkhorshid, E.; Schulten, K. *J. Chem. Phys.* **2003**, *119* (6), 3559−3566.
(40) Israelachvili, J. N. *Intermolecular and surface forces*, revised 3rd ed. Academic Press: San Diego, CA, 2011.
(41) Müller-Plathe, F. *ChemPhysChem* **2002**, *3* (9), 754−769.
(42) Reith, D.; Putz, M.; Muller-Plathe, F. *J. Comput. Chem.* **2003**, *24* (13), 1624−36.
(43) Tsige, M.; Taylor, P. L. *Phys. Rev. E* **2002**, *65* (2Pt 1), 021805.
(44) Jarzynski, C. *Phys. Rev. Lett.* **1997**, *78* (14), 2690−2693.
(45) Park, S.; Schulten, K. *J. Chem. Phys.* **2004**, *120* (13), 5946−5961.

(46) Leach, A. R.; Schomburg, D. *Molecular modelling: principles and applications*; Longman: London, 1996.
(47) Forrest, J. A.; Dalnoki-Veress, K.; Stevens, J. R.; Dutcher, J. R. *Phys. Rev. Lett.* **1996**, *77*, 2002−2005.
(48) Sharp, J. S.; Forrest, J. A. *Phys. Rev. Lett.* **2003**, *91* (23), 235701.
(49) Ellison, C. J.; Torkelson, J. M. *Nat. Mater.* **2003**, *2* (10), 695−700.
(50) Reiter, G. *Langmuir* **1993**, *9* (5), 1344−1351.
(51) Rose, J. H.; Ferrante, J.; Smith, J. R. *Phys. Rev. Lett.* **1981**, *47* (9), 675−678.
(52) Rose, J. H.; Smith, J. R.; Ferrante, J. *Phys. Rev. B* **1983**, *28* (4), 1835−1845.
(53) Banerjea, A.; Smith, J. R. *Phys. Rev. B* **1988**, *37* (12), 6632−6645.
(54) de Boer, J. H. *Trans. Faraday Soc.* **1936**, *32* (0), 10−37.
(55) Hamaker, H. C. *Physica* **1937**, *4* (10), 1058−1072.
(56) Rubinstein, M.; Colby, R. H. *Polymer Physics*; OUP: Oxford, U.K., 2003.
(57) Balzer, B. N.; Micciulla, S.; Dodoo, S.; Zerball, M.; Gallei, M.; Rehahn, M.; v. Klitzing, R.; Hugel, T. *ACS Appl. Mater. Interfaces* **2013**, *5* (13), 6300−6306.
(58) Shin, K.; Obukhov, S.; Chen, J. T.; Huh, J.; Hwang, Y.; Mok, S.; Dobriyal, P.; Thiyagarajan, P.; Russell, T. P. *Nat. Mater.* **2007**, *6* (12), 961−965.
(59) Jones, R. L.; Kumar, S. K.; Ho, D. L.; Briber, R. M.; Russell, T. P. *Nature* **1999**, *400* (6740), 146−149.
(60) Hanakata, P. Z.; Douglas, J. F.; Starr, F. W. *Nat. Commun.* **2014**, *5*, 4163.